

Supporting information

Integrating smartphone-assisted ratiometric fluorescent sensor with in-situ hydrogel extraction for visual detection of organophosphorus pesticides

Xia Tong,^{a,b} Guihan Cai,^a Yongfeng Zhu,^a Chaoying Tong,^a Fang Wang,^b Ying Guo,^{c,*}
Shuyun Shi,^{a,b,*}

^a College of Chemistry and Chemical Engineering, Central South University, Changsha 410083, Hunan, China

^b Key Laboratory of Modern Preparation of Traditional Chinese Medicine under Ministry of Education, Jiangxi University of Traditional Chinese Medicine, Nanchang 330004, Jiangxi, China

^c Department of Clinical Pharmacology, Xiangya Hospital, Hunan Key Laboratory of Pharmacogenetics, Central South University, Changsha, 410078, Hunan, China.

*Corresponding author: Tel./fax: +86 731 88879616.

E-mail address: shuyshi@csu.edu.com (S. Shi).

Experiment section

Materials and apparatus

Cucumber, strawberry and cherry tomato were purchased from a local market (Changsha, China). Acetylcholinesterase (AChE; EC 3.1.1.7) from fly head, alkaline phosphatase (ALP; EC 3.1.3.1), α -glucosidase (α -Glu) and acetylthiocholine (ATCh) were obtained from Yuanye Bio-Technology Co., Ltd (Shanghai, China). 2-[4-(2-hydroxyethyl)piperazin-1-yl]ethanesulfonic acid (HEPES), polyoxyethylene bis(amine) ($\text{H}_2\text{N-PEG-NH}_2$, MW: 2000, degree of polymerization (DP): 76) were brought from Aladdin (Shanghai, China). Acetonitrile, formic acid, methanol, ethanol, *o*-phenylenediamine (OPD), parathion-methyl, dichlorvos, parathion, dimethoate, glyphosate calcium gluconate, sodium alginate (SA), 2,4-dichlorophenoxyacetic acid (2,4-D), fipronil, thiram, glycine (Gly), serine (Ser), glucose (Glu), HCl, NaOH, H_2SO_4 , NaCl, KCl, AgNO_3 , CaCl_2 , MgSO_4 , $\text{Zn}(\text{NO}_3)_2$ and AlCl_3 were provided from Sinopharm Chemical Reagent Co., Ltd (Beijing, China). Ultrapure water was from molecular water purification system (18.25 M Ω -cm). All reagents were analytical reagent grade.

The morphologies and sizes of carbon dots (CDs) were measured by a Tecnai G2 20S-Twin transmission electron microscope (TEM, FEI, Prague, Czech) with an accelerating voltage of 200 kV. The morphologies of SA hydrogel were characterized using field-emission scanning electron microscopy (SEM, S-4800, Hitachi, Tokyo, Japan). X-ray photoelectron spectroscopy (XPS) was characterized with Escalab Xi+ (Thermo Fisher Scientific, USA). X-ray diffraction (XRD) was taken on Bruker D8 Advance (Bruker, Germany). Ultraviolet-visible (UV-vis) absorption spectra were obtained on a UV-2600 UV-vis spectrophotometer (Shimadzu, Japan). Fourier transform infrared (FT-IR) spectra were performed by Spectrum Two (PerkinElmer

Ltd., USA). The fluorescence decay time curves were collected on a Fluo Time 100 spectrofluorometer (PicoQuant, Germany). The fluorescent spectra were measured by a LS-55 spectrofluorometer (PerkinElmer Ltd., USA) with a voltage of 850 V under 365 nm excitation, the wavelength range of 385–720 nm, and slit width of 15 nm and 20 nm for excitation and emission spectra.

Quantum yield measurements

Quantum yield (QY) of CDs was calculated by the following equation:

$$QY_{sam} = QY_{ref} \frac{I_{sam} A_{ref} n_{sam}^2}{I_{ref} A_{sam} n_{ref}^2}$$

Where QY is quantum yield, I represents integrated fluorescence intensity, A is optical density, n is the refractive index of solvent, sam and ref denote sample and reference standard. QY of quinine sulfate was 0.58 at 360 nm (0.1M H₂SO₄) as reference standard for CDs [1].

IFE correction by Parker model

IFE can be estimated according to Parker model [2]:

$$\frac{F_{cor}}{F_{obsd}} = \frac{2.3dA_{ex}}{1 - 10^{-dA_{ex}}} 10gA_{em} \frac{2.3sA_{em}}{1 - 10^{-sA_{em}}}$$

Where, F_{obsd} is the measured fluorescence intensity of fluorophore and F_{cor} is the corrected fluorescence intensity by removing IFE from F_{obsd} . A_{ex} and A_{em} denote the absorbance at the excitation and emission wavelength, respectively. d represents the width of the cuvette (1.00 cm), g is the distance between the edge of the excitation beam and the cuvette (0.40 cm), and s is the thickness of excitation beam (0.10 cm). All the tests are conducted in triplicate.

Procedure for Ag⁺ detection

Briefly, OPD (0.1 M, 75 μ L) and different concentration of Ag⁺ were added into HEPES solution (1.4 mL, 10 mM, pH 8.0), and incubated for 15 min at 37°C. CDs solution (15 mg mL⁻¹, 15 μ L) was added into the above solution. The fluorescent spectra were collected at 365 nm excitation *via* fluorescent spectrophotometer, and the fluorescent images were captured by smartphone-assisted platform.

Procedure for AChE activity detection

Various AChE activity was incubated with ATCh (4.5 mM, 10 μ L) in HEPES solution (1.4 mL, 10 mM, pH 8.0) for 35 min at 37°C. Following this, Ag⁺ (10 mM, 5 μ L) was added and incubated for 10 min at 37°C. Then, OPD (0.1 M, 75 μ L) was added into solution at 37°C for 15 min, and CDs was introduced into reaction solution. The fluorescent spectra were recorded at 365 nm excitation *via* fluorescent spectrophotometer, and the fluorescent images were captured by smartphone-assisted platform.

Selectivity tests for parathion-methyl

The selectivity and anti-interference tests of AChE/ATCh/Ag⁺/OPD/CDs system for OPs were investigated. Some substances, including Na⁺, K⁺, Ca²⁺, Mg²⁺, Al³⁺, glycine (Gly), serine (Ser), glucose (Glu), alkaline phosphatase (ALP), α -Glu (α -glucosidase), other kinds of pesticides (2,4-dichlorophenoxyacetic acid (2,4-D), fipronil, thiram) were applied. The final concentrations of Na⁺, K⁺, Ca²⁺, Mg²⁺, Al³⁺, Gly, Ser, Glu were set at 50 μ M, ALP and α -Glu activity are 100 U·L⁻¹, 2,4-D, fipronil and thiram concentration were 30 μ g·L⁻¹, and dichlorvos, parathion, dimethoate,

glyphosate and parathion-methyl concentration were $30 \mu\text{g}\cdot\text{L}^{-1}$. In selectivity tests, the above-mentioned substances were introduced into reaction system without parathion-methyl, respectively. In anti-interference tests, parathion-methyl was mixed with these substances, respectively. The subsequent procedures were the same with those in detection of OPs.

HPLC–MS system for parathion-methyl analysis

High performance liquid chromatography (HPLC) analysis was conducted on an Agilent 1260 HPLC system with UV detector at 278 nm (Agilent Technologies, Santa Clara, CA). A Waters SunFire-C₁₈ chromatographic column (250 nm × 4.6 mm i.d., 5 μm, Waters, Milford, MA) was selected for separation at 30°C. The mobile phase consisted of 0.1% formic acid in ultrapure water (A) and methanol (B) was used as mobile phase for isocratic elution (0–15 min, 70% B). A flow rate of $0.8 \text{ mL}\cdot\text{min}^{-1}$ was employed for elution and the injected sample volume was set at 20 μL. Bruker compact QTOF-MS (Quadrupole-time of flight-mass spectrometry) system with electrospray ionization (ESI) ion source was used for MS data acquisition. The optimal parameters for parathion-methyl identification in positive ion mode were set as follows: scan range was 100–1000 m/z with spray voltage at 3.5 kV, flow rate of dry gas was 8.0 L/min with temperature at 200°C, nebulizer pressure was 35 psi.

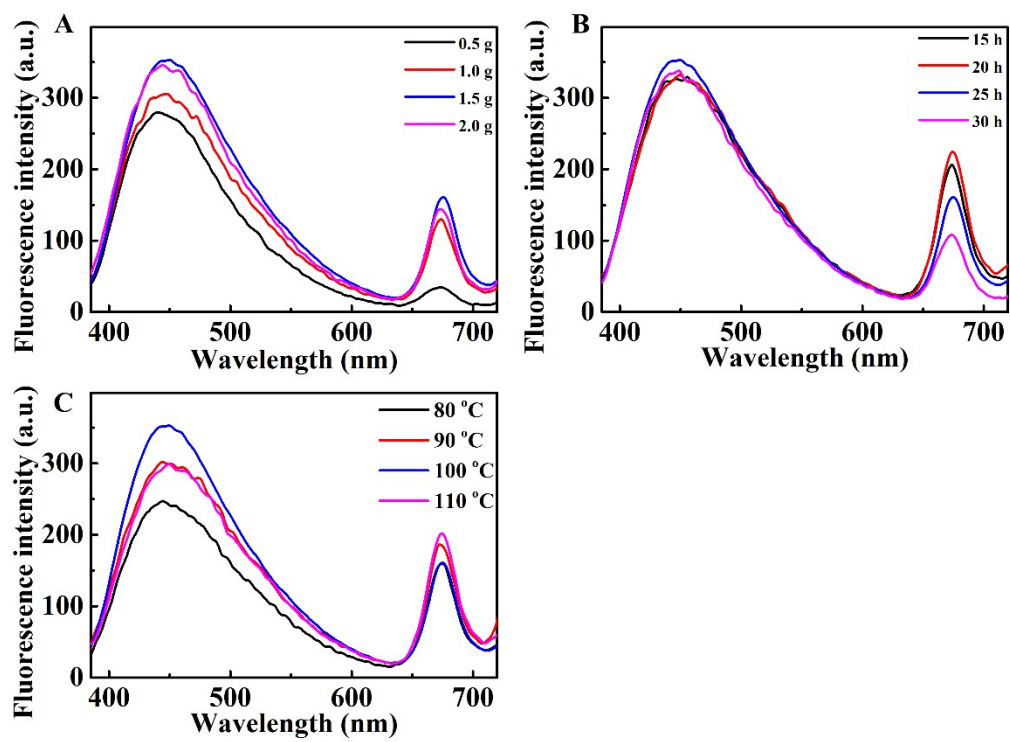


Fig. S1 The fluorescence intensity of CDs under (A) different mass of cucumber, (B) reaction time and (C) synthesis temperature.

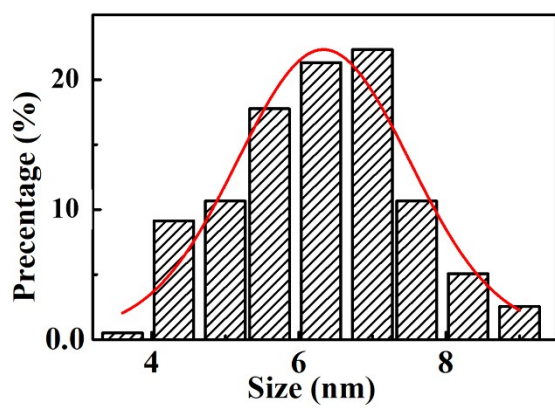


Fig. S2 The size distribution of CDs from TEM image.

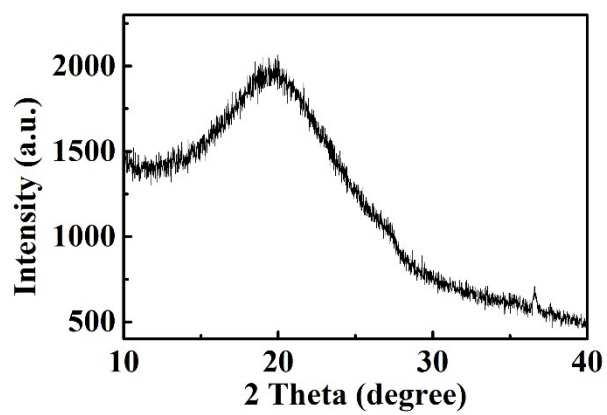


Fig. S3 XRD pattern of CDs.

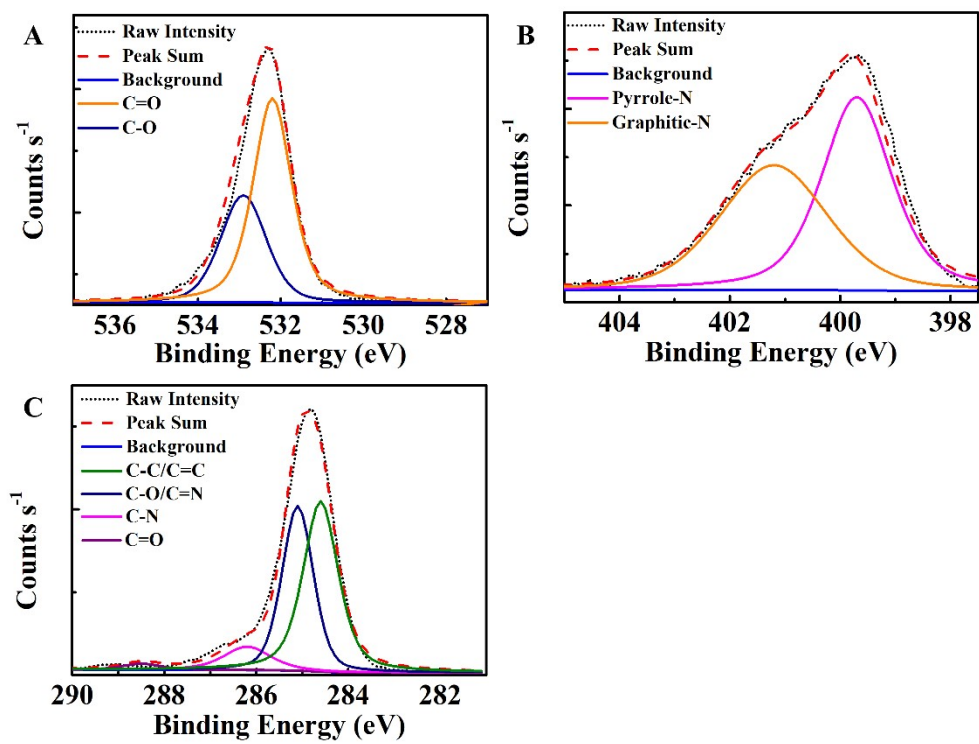


Fig. S4 High-resolution XPS spectra of (A) O 1s, (B) N 1s, (C) C 1s of CDs.

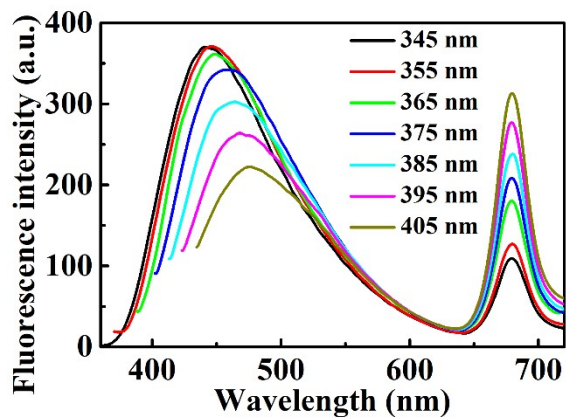


Fig. S5 Fluorescent emission spectra of CDs under different excitation wavelengths (345, 355, 365, 375, 385, 395 and 405 nm).

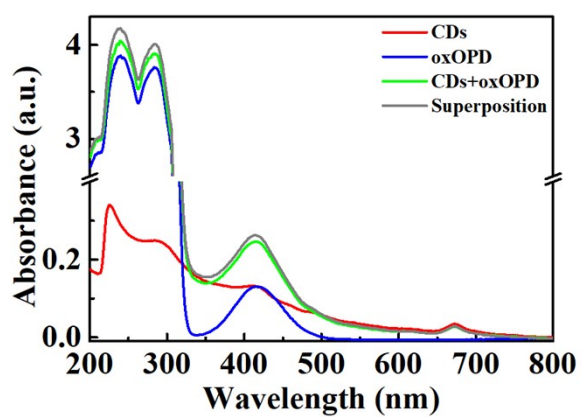


Fig. S6 UV-vis absorption spectra of CDs, oxOPD, CDs+oxOPD and the superposition spectrum of CDs and oxOPD.

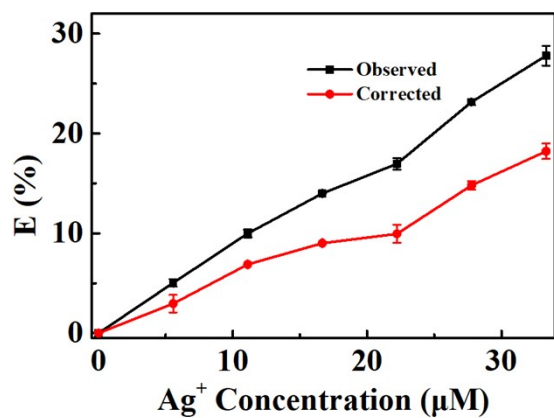


Fig. S7 The observed and corrected suppressed efficiency (E (%)) of oxOPD on the fluorescence of CDs.

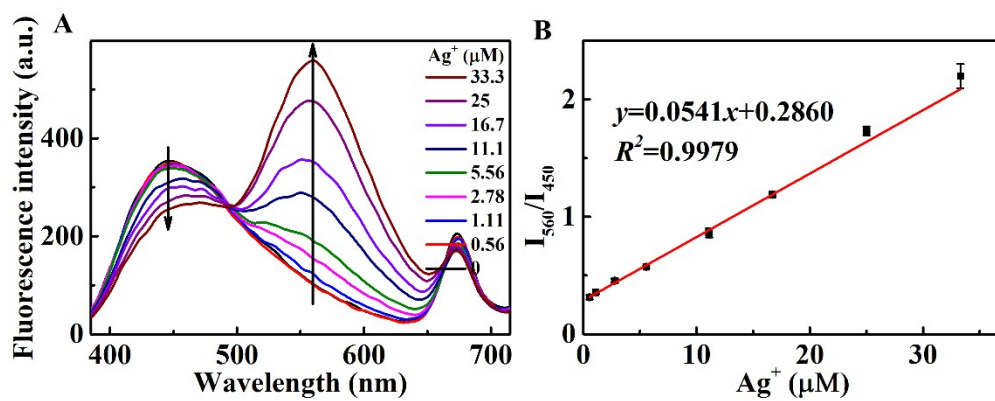


Fig. S8 (A) Fluorescent spectra of OPD/CDs with different concentration of Ag^+ . (B) Linear fitting curve of I_{560}/I_{450} ratio versus Ag^+ concentration (0.6, 1.1, 2.8, 5.7, 11.1, 16.7, 25.0 and 33.3 μM).

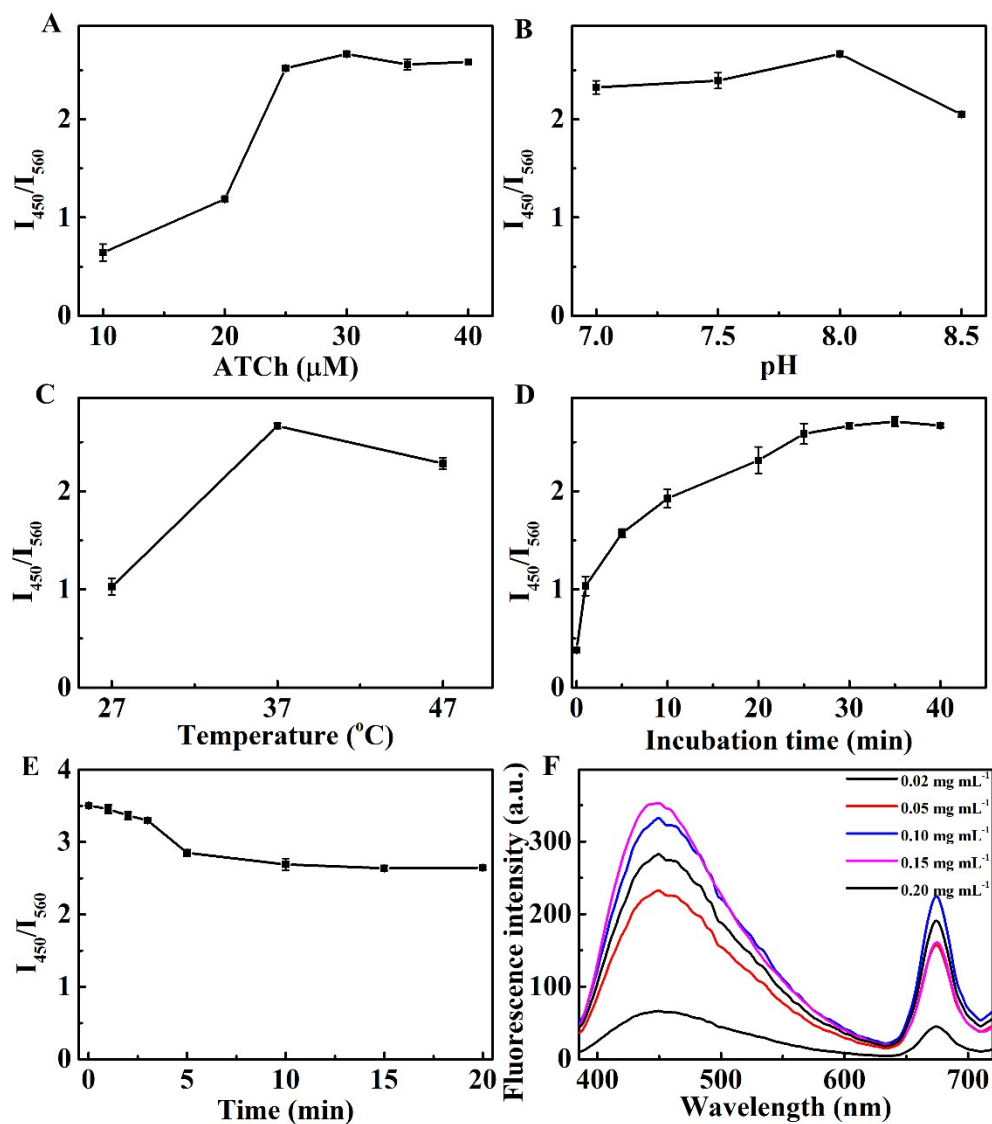


Fig. S9 The effects of (A) ATCh concentration, (B) pH, (C) enzymatic temperature, (D) incubation time between ATCh and AChE, (E) incubation time between Ag⁺ and OPD on AChE/ATCh/Ag⁺/OPD/CDs system in the presence of AChE activity (14 U·L⁻¹). (F) The fluorescent spectra of CDs under different concentration.

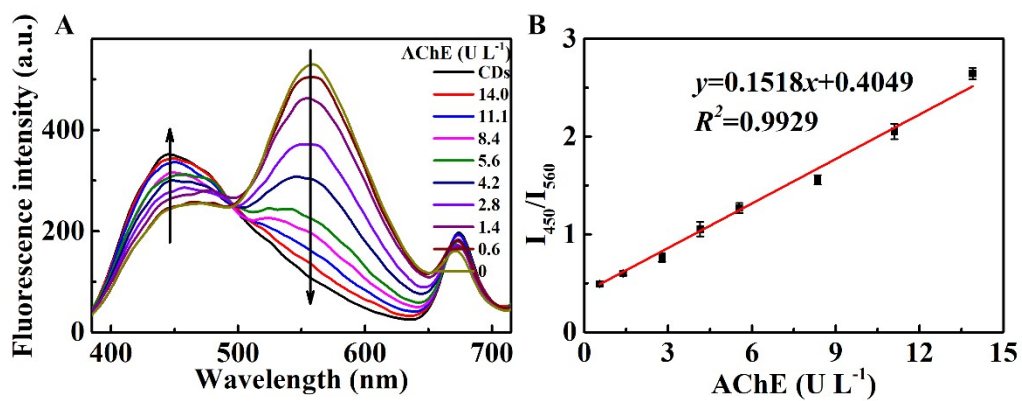


Fig. S10 (A) Fluorescent spectra of AChE/ATCh/Ag⁺/OPD/CDs system in the presence of different AChE activity. (B) Linear fitting curve of I₄₅₀/I₅₆₀ ratio versus AChE activity (0.6, 1.4, 2.8, 4.2, 5.6, 8.4, 11.1 and 14.0 U·L⁻¹).

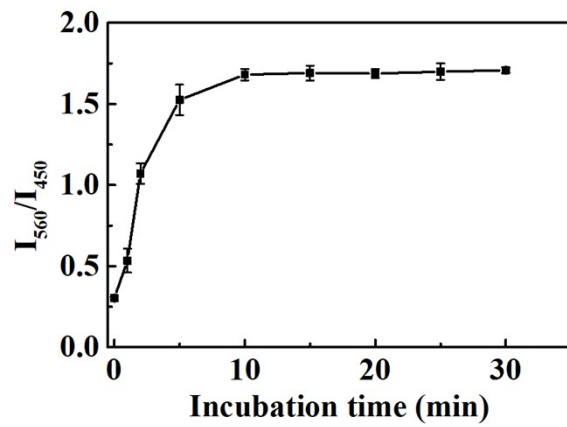


Fig. S11 The reaction time between parathion-methyl and AChE.

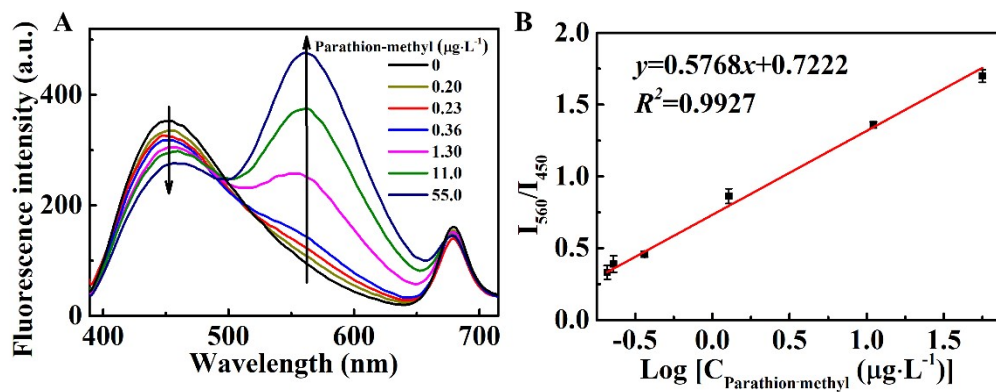


Fig. S12 (A) The fluorescent spectra of AChE/ATCh/Ag⁺/OPD/CDs system with the increment of parathion-methyl concentration. (B) Linear fitting curve of I_{560}/I_{450} ratio versus the logarithm of parathion-methyl concentration (0.20, 0.23, 0.36, 1.30, 11.0 and 55.0 $\mu\text{g}\cdot\text{L}^{-1}$).

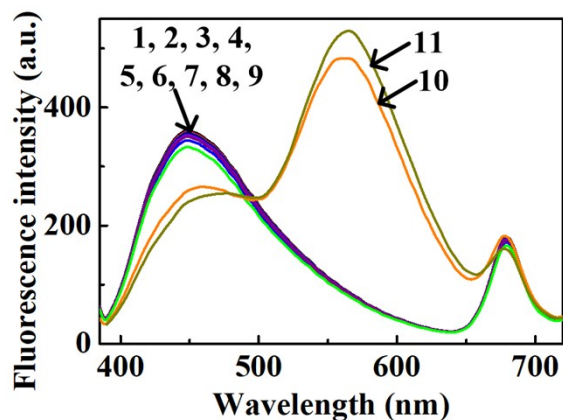


Fig. S13 Fluorescent spectra of (1) CDs, (2) AChE/CDs, (3) OPD/CDs, (4) AChE/ATCh/CDs, (5) parathion-methyl/AChE/CDs, (6) parathion-methyl/AChE/ATCh/CDs, (7) AChE/ATCh/Ag⁺/CDs, (8) parathion-methyl/AChE/ATCh/Ag⁺/CDs, (9) AChE/ATCh/Ag⁺/OPD/CDs, (10) parathion-methyl/AChE/ATCh/Ag⁺/OPD/CDs and (11) Ag⁺/OPD/CDs.

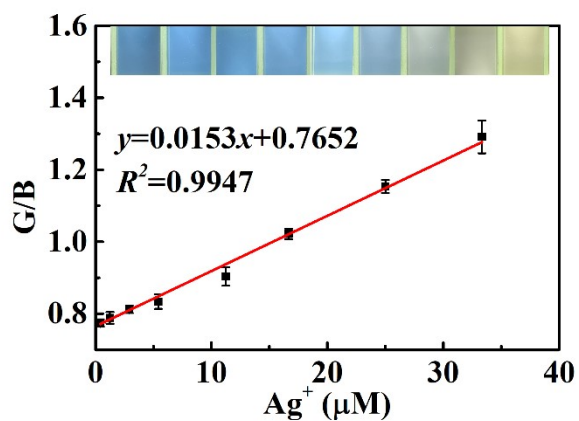


Fig. S14 Linear relationship between G/B ratio of photographs versus Ag⁺ concentration (0.6, 1.1, 2.8, 5.7, 11.1, 16.7, 25.0, 33.3 µM) (insets: the photographs of Ag⁺/OPD/CDs system recording with smartphone-assisted platform in the presence of Ag⁺ (0, 0.6, 1.1, 2.8, 5.7, 11.1, 16.7, 25.0, 33.3 µM)). Error bars represent standard deviations (n=3).

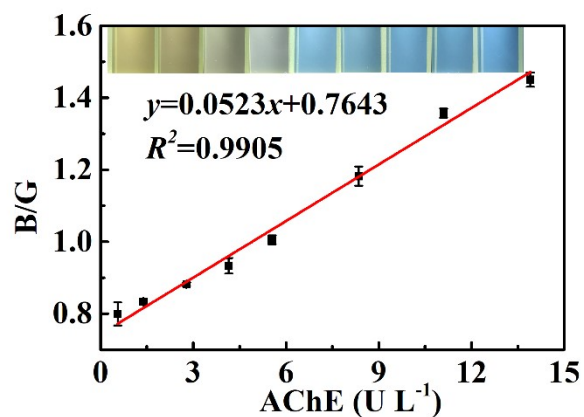


Fig. S15 Linear relationship between B/G ratio of the photographs versus AChE activity (0.6, 1.4, 2.8, 4.2, 5.6, 8.4, 11.1 and 14.0 U·L⁻¹) (insets: the photographs of AChE/ATCh/Ag⁺/OPD/CDs system recording with smartphone-assisted platform in the presence of AChE (0, 0.6, 1.4, 2.8, 4.2, 5.6, 8.4, 11.1 and 14.0 U·L⁻¹)). Error bars represent standard deviations (n=3).

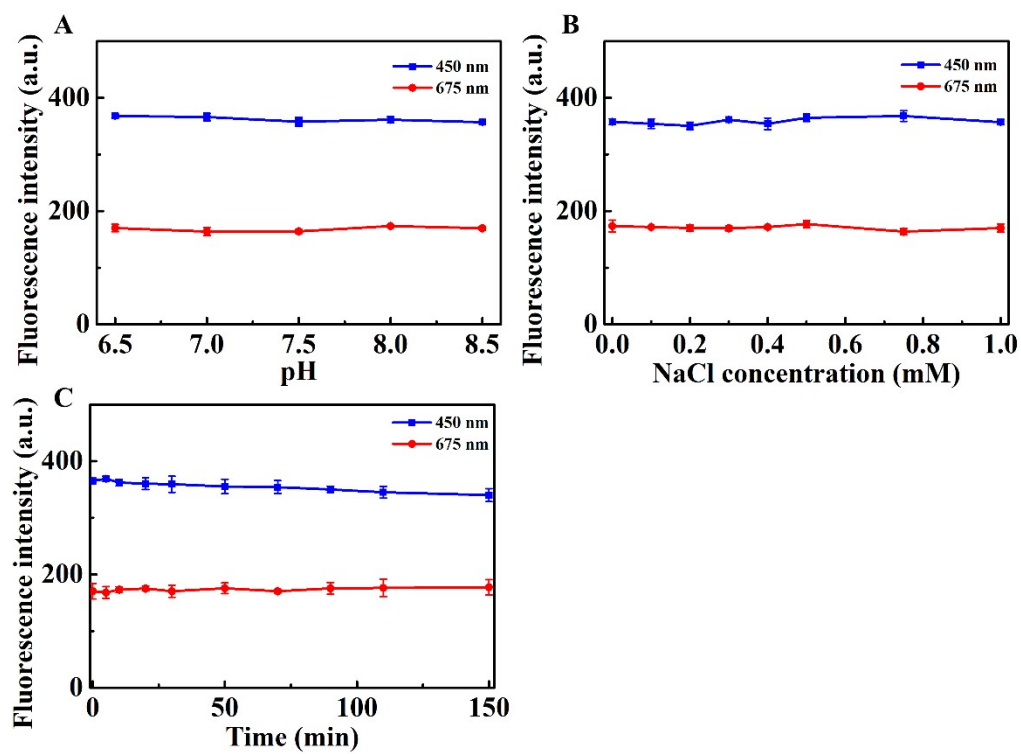


Fig. S16 The effects of (A) pH, (B) NaCl concentration and (C) UV irradiation time (365 nm) on fluorescence intensity of CDs.

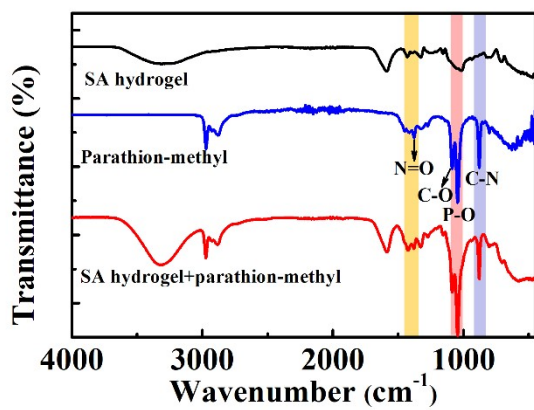


Fig. S17 FT-IR spectra of SA hydrogel, parathion-methyl and SA hydrogel/parathion-methyl.

Table S1. IFE of oxOPD on the fluorescence of CDs.

Ag^+ (μM)	A_{ex}	A_{em}	CF	F_{obsd}	F_{cor}	$F_{cor,0}/F_{cor}$
0	0.119	0.078	1.24	358.05	442.80	1
5.6	0.126	0.092	1.26	340.02	429.70	1.03
11.1	0.129	0.101	1.28	322.285	412.24	1.07
16.7	0.134	0.117	1.31	307.935	402.87	1.10
22.2	0.140	0.130	1.34	296.64	396.15	1.12
27.8	0.148	0.147	1.37	275.15	377.21	1.17
33.3	0.159	0.152	1.39	257.94	359.75	1.23

Table S2. The individual ranges of the various OPs.

Type	Linear range ($\mu\text{g L}^{-1}$)	Linear equation	LOD ($\mu\text{g L}^{-1}$)
Dichlorvos	0.5–30	$y=0.4610\text{Log } [C]+0.8101$ (R^2 0.9905)	0.20
Parathion	1.0–50	$y=0.3809\text{Log } [C]+0.8351$ (R^2 0.9895)	0.30
Dimethoate	5.0–200	$y=0.2684\text{Log } [C]+0.8324$ (R^2 0.9923)	1.0
Glyphosate	2.0–100	$y=0.3496\text{Log } [C]+0.8257$ (R^2 0.9942)	0.50

Table S3. Comparison of reported methods for OP detection.

Methods	In situ extraction/On-site measurement	OPs	LOD ($\mu\text{g}\cdot\text{L}^{-1}$)	Ref.
SERS ¹	Yes/Yes	Parathion-methyl	0.1	[3]
Electrochemical method	Yes/Yes	Parathion-methyl	2.63	[4]
N-CDs-based fluorescent method	No/No	Parathion-methyl	0.013	[5]
		Dichlorvos	0.003	
SiQDs-based fluorescent method	No/Yes	Paraoxon	10	[6]
GQDs@Tb/GMP ICP-based fluorescent method ²	No/Yes	Parathion	0.037	[7]
CuNPs/Urease/Urea fluorescent method	No/Yes	Dimethoate	1.0	[8]
rQDs@SiO ₂ @gQDs probe ³	No/Yes	Glyphosate	0.48	[9]
CDs-based fluorescent method	Yes/Yes	Parathion-methyl	0.50	This work
		Dichlorvos	0.20	
		Parathion	0.30	
		Dimethoate	1.0	
		Glyphosate	0.50	

¹ Surface-enhanced Raman scattering

² Graphene quantum dot (GQD)-sensitized terbium/guanine monophosphate (Tb/GMP) infinite coordination polymer (ICP)

³ Red-emission quantum dots@SiO₂ nanoparticles@green-emission quantum dots

Table S4. Determination and recovery tests of parathion-methyl in strawberry and cherry tomato samples by HPLC–MS.

	Spiked ($\mu\text{g}\cdot\text{L}^{-1}$)	Found ($\mu\text{g}\cdot\text{L}^{-1}$)	Recoveries (%)	RSD (%)
Strawberry	0	ND ^a	–	–
	3.00	2.83±0.16	94.3	5.6
	20.0	22.5±0.47	112.5	2.1
	40.0	40.2±1.49	98.2	3.7
Cherry tomato	0	ND	–	–
	5.00	5.03±0.16	100.6	3.2
	30.0	28.6±0.14	91.3	4.8
	50.0	51.2±3.48	102.4	6.8

^a Not detected

References

- [1] S. Lu, G. Li, Z. Lv, N. Qiu, W. Kong, P. Gong, G. Chen, L. Xia, X. Guo, J. You. Facile and ultrasensitive fluorescence sensor platform for tumor invasive biomarker β -glucuronidase detection and inhibitor evaluation with carbon quantum dots based on inner-filter effect. *Biosensors and Bioelectronics* 85 (2016) 358–362.
- [2] X. Tong, S. Shi, C. Tong, A. Iftikhar, R. Long, Y. Zhu, Quantum/carbon dots-based fluorescent assays for enzyme activity, *TrAC Trends in Analytical Chemistry* 131 (2020) 116008
- [3] W. Fang, X. Zhang, Y. Chen, L. Wan, W. Huang, A. Shen, J. Hu. Portable SERS-enabled micropipettes for microarea sampling and reliably quantitative detection of surface organic residues. *Analytical chemistry* 87(18) (2015) 9217–9224.
- [4] F. Zhao, J. He, X. Li, Y. Bai, Y. Ying, J. Ping. Smart plant-wearable biosensor for in-situ pesticide analysis. *Biosensors and Bioelectronics* 170 (2020) 112636.
- [5] S. Huang, J. Yao, X. Chu, Y. Liu, Q. Xiao, Y. Zhang. One-step facile synthesis of nitrogen-doped carbon dots: a ratiometric fluorescent probe for evaluation of acetylcholinesterase activity and detection of organophosphorus pesticides in tap water and food. *Journal of Agricultural and Food Chemistry* 67(40) (2019) 11244–11255.
- [6] R. Jin, D. Kong, X. Yan, X. Zhao, H. Li, F. Liu, P. Sun, Y. Lin, G. Lu. Integrating target-responsive hydrogels with smartphone for on-site ppb-level quantitation of organophosphate pesticides. *ACS Applied Materials & Interfaces* 11(31) (2019) 27605–27614.
- [7] R. Ma, M. Xu, C. Liu, G. Shi, J. Deng, T. Zhou. Stimulus response of GQD-sensitized Tb/GMP ICP nanoparticles with dual-responsive ratiometric fluorescence: toward point-of-use analysis of acetylcholinesterase and organophosphorus pesticide poisoning with acetylcholinesterase as a biomarker. *ACS Applied Materials &*

Interfaces 12(37) (2020) 42119–42128.

[8] D. Kong, R. Jin, T. Wang, H. Li, X. Yan, D. Su, C. Wang, F. Liu, P. Sun, X. Liu, Y. Gao, J. Ma, X. Liang, G. Lu. Fluorescent hydrogel test kit coordination with smartphone: robust performance for on-site dimethoate analysis. *Biosensors and Bioelectronics* 145 (2019) 111706.

[9] D. Wei, Y. Wang, N. Zhu, J. Xiao, X. Li, T. Xu, X. Hu, Z. Zhang, D. Yin. A Lab-in-a-Syringe device integrated with a smartphone platform: colorimetric and fluorescent dual-mode signals for on-site detection of organophosphorus pesticides. *ACS Applied Materials & Interfaces* 13(41) (2021) 48643–48652.